minerals

MDPI

Article

Characterization of Historic Lime Mortars from the Arch of San Martin to Identify the Construction Phases of the City Wall of Burgos (Spain)

Graciela Ponce-Antón [1], Maria Cruz Zuluaga [1], Luis Ángel Ortega [1,*], Javier Jiménez Echevarría [2] and Carmen Alonso Fernández [2]

[1] Department of Geology, University of the Basque Country (UPV/EHU), Sarriena s/n, 48940 Leioa, Spain; graciela.ponce@ehu.eus (G.P.-A.); mcruz.zuluaga@ehu.eus (M.C.Z.)
[2] Cronos S.C. Arqueología y Patrimonio, C/Aparicio y Ruíz 16, 4, 09003 Burgos, Spain; jj@cronossc.es (J.J.E.); ca@cronossc.es (C.A.F.)
* Correspondence: luis.ortega@ehu.eus

Abstract: Historical lime mortars provide valuable information on the construction phases of buildings and allow reconstruction of the chronology of the historical structures. The City Wall of Burgos and the Mudejar Arch of San Martin were declared an Asset of Cultural Interest and have been protected since 1949. Several restorations at the end of the 20th century altered the original appearance of the wall and the current gate, making it difficult to establish stratigraphic relationships between the two structures. Given the scarcity of information on the construction phases of the wall and the uncertainty of the historical dates, a mineralogical and chemical characterization of the mortars was carried out, and the suitability of the binder for radiocarbon dating was assessed. The petrographic, mineralogical and chemical analyses of the lime mortars from the Arc of San Matin show distinctive characteristics, suggesting different construction periods and production processes, where the selection of raw materials and production methods was conducted according to the construction requirements. Moreover, the presence of contaminant phases and microparticles of charcoal in the binder fraction led to discard all the samples for mortar radiocarbon dating.

Keywords: mineralogy; lime mortar; binder; integrated analyses

Citation: Ponce-Antón, G.; Zuluaga, M.C.; Ortega, L.Á.; Jiménez Echevarría, J.; Alonso Fernández, C. Characterization of Historic Lime Mortars from the Arch of San Martin to Identify the Construction Phases of the City Wall of Burgos (Spain). *Minerals* **2024**, *14*, 147. https://doi.org/10.3390/min14020147

Academic Editor: Alberto De Bonis

Received: 15 December 2023
Revised: 24 January 2024
Accepted: 28 January 2024
Published: 29 January 2024

1. Introduction

One of the main goals of architectural archaeology with regard to historic buildings is to provide information on construction phases and to reconstruct the chronology of buildings (e.g., [1–8]). However, this information is not always easy to obtain, as usually the construction information is scarce or historical documents are not available.

The archaeometric study of mortars provides information that allows us to understand the technologies used to make mortars in the past, to identify the raw materials and their provenance issues and to recognize the construction phases of a building [4,9–12]. The study of old mortars also has an important role in formulating compatible mortars for restoration works [13–18].

To establish the chronology of the construction phases of the buildings. absolute dating of the lime mortars is mainly used. In radiocarbon dating of mortars, the charcoal embedded in the mortar (e.g., [19–27]) or the lime binder (e.g., [28–34]) are used. Nevertheless, the use of charcoal fragments should be used with caution due to the effects of old wood [35]. The lime mortar dating method consists of isolating the high-purity binder fraction by extracting specific grain size fractions from the mortar, avoiding contaminants. Geological carbonates and the newly formed carbonated mineral phases during the manufacture of mortars are the most common contaminants, leading to overestimating radiocarbon

dates. Secondary carbonates formed during alteration processes also lead to underestimation of the radiocarbon ages [31,36,37]. To avoid contaminants, several techniques are proposed to separate the pure binder fraction, including mechanical [30,31,34,38] and chemical separation methods [29,39–41]. Thus, an appropriate chemical and mineralogical characterization of both the bulk mortar and the isolated binder fraction greatly enhances the understanding of mortar features and allows a reliable preliminary assessment of the binder for radiocarbon dating.

The City Wall of Burgos (Spain) is classified as an Asset of Cultural Interest in the category of Castle, under the protection of the General Declaration of the Decree of 22nd April 1949 (B.O.E. No. 125, of 5th May 1949 and Law 16/1985 on the Spanish Historical Heritage). This decree applies to all castles in Spain, regardless of their state of conservation, and prevents any intervention that could alter them or lead to their collapse. Since 2014, the Wall of Burgos has been a structure with integral protection in the General Urban Development Plan of the city of Burgos under the category of "Historic-Artistic Site".

The construction of the medieval Wall of Burgos dates back to the reign of Alfonso X (1252–1284), although earlier documents mention a fence from dating from the end of the 11th century. However, the dates are imprecise, and not all the fabrics are homogeneous in terms of construction, nor necessarily contemporary. The construction of the Arch of San Martin dates back to 1375, although in 1740 partial demolition was reported. The relevance of the Arch of San Martín lies in the fact that until the 16th century, it was the main entrance to the city of Burgos. It takes its name from the nearby church of San Martín, which is no longer present. This gate is a Mudejar-style horseshoe arch flanked by two sturdy semi-circular cubes, which differ in appearance between the north and south cubes, with the latter being heavily modified at the base. The current gate underwent several restorations at the end of the 20th century, changing its original appearance.

The city walls are complex historical constructions, characterized by the overlapping of different types of masonry, due to the addition of structural elements and refurbishment works over time. The aims of the present work are to determine the construction phases close to the Arch of San Martin in the city wall of Burgos on the basis of the mineralogical and chemical characterization of the lime mortars and also to evaluate the suitability of the lime mortars for radiocarbon dating.

2. Materials and Methods

2.1. Materials

The city Wall of Burgos is classified as an Asset of Cultural Interest, and therefore the mortar sampling was limited. The mortar samples were carefully selected based on the interpretation of the architectural sequence, since the exact dates of the constructive phases were unknown. Thus, three samples were collected (Table 1, Figure 1). Sample ARC-1 (11th century) corresponds to a whitish mortar joining eroded and broken sandstone ashlars from the foundations of a circular cube. Sample ARC-2 (first half of the 13th century) corresponds to the foundation of a quadrangular cube built over the circular cube and joins squared ashlars of sandstone and limestone. Sample ARC-3 (second half of the 13th century) corresponds to the intrados of the Mudejar arch.

Table 1. Sample location.

Sample	SU	Structure	Broad Age Range
ARC-1	UE213	Foundation of the circular cube	11th century
ARC-2	UE210	Quadrangular foundation, covering the circular cube foundation	First half of the 13th century
ARC-3	-	Intrados of the Mudejar arch	Second half of the 13th century

SU: Stratigraphic Unit.

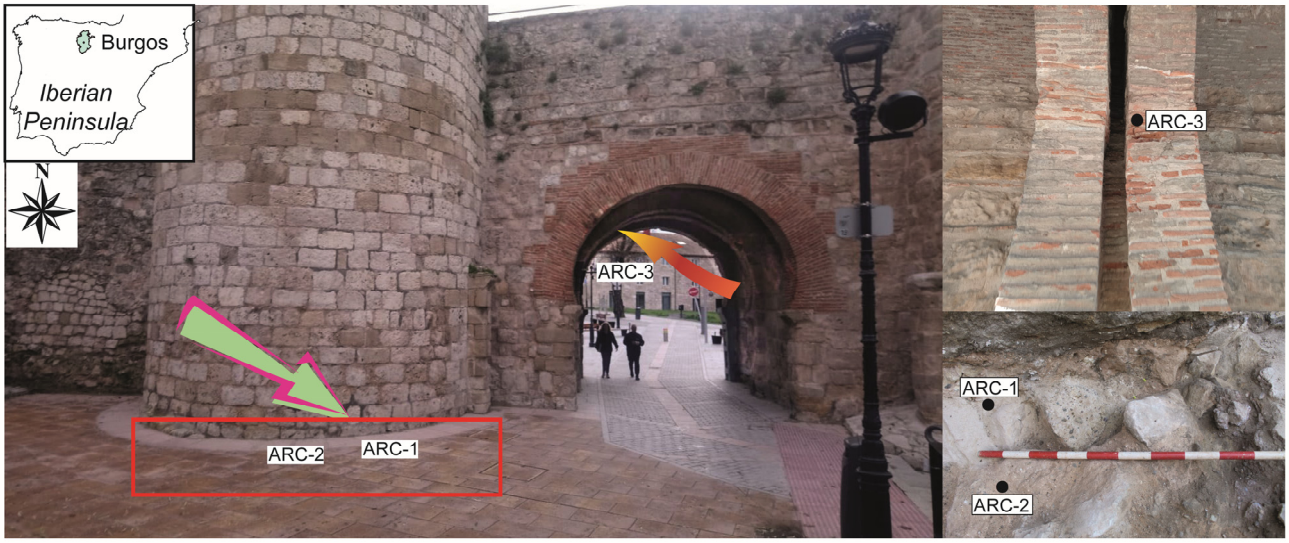

Figure 1. Sample location at the Arch of San Martin (Burgos, Spain). Arrows indicate sampling sites. Currently the ARC-1 and ARC-2 sampling site is covered.

In order to assess the suitability of the lime mortars for radiocarbon dating, a binder fraction of each sample was characterized. The lime binder fraction was extracted by settling following the procedure described by [30,31]. To characterize the binder, the binder fractions with particle size <20 μm and <2 μm were considered.

2.2. Methods

The microtexture and mineralogical nature of the mortar components were determined on polished thin sections using a Nikon Eclipse LV100POL optical polarizing microscope equipped with DS F-I1 digital camera and a DS L-2 control unit, in both transmitted and reflected polarized light modes. A comparison chart for visual percentage estimation was used to define the mortar binder/aggregate ratios at the Laboratory of the Department of Geology, University of the Basque Country (UPV/EHU). Binder/aggregate ratios were defined using a comparison chart for visual percentage estimation [42].

Mineralogical analyses were performed using X-ray diffraction (XRD) analysis of powder samples using a Philips X'Pert diffractometer (Malvern PANalytical, Almelo, The Netherlands) equipped with a monochromatic Cu-kα1 X-radiation operating at 40 kV and 20 mA. The data collection on the powder sample was performed by a continuous scan in the range 5–70 °2θ, at an acquisition rate of 0.02 grade per second 2θ. Interpretation of diffraction patterns and semi-quantitative calculations were performed with X'Pert High-Score Plus 3.0 software by PANalytical (Malvern PANalytical, Almelo, The Netherlands), on the basis of the characteristic space of each mineral, reconstructing the mineral profiles of the compounds and comparing the experimental peaks with experimental patterns of ICDD and ICSD diffraction databases.

The elemental chemical composition of major elements of mortars was determined by means of X-ray Fluorescence (XRF) using a Wavelength Dispersive X-ray Fluorescence (WDXRF) PANalytical Axios Advanced PW4400 XRF spectrometer with 4 kW Rh anode SST-mAX X-ray tube with a detection limit of 0.01 wt%. Fused beads were obtained by melting the powder bulk mortar sample with lithium borate flux (Spectromelt A12, Merck, Darmstadt, Germany) in 20:1 proportion at 1200 °C for 3 min in Pt/Au crucibles using a PANalytical Perl'X3. The loss on ignition (LOI) was calculated after heating the powder bulk mortar sample at 1050 °C for one hour.

The binder fractions were also analyzed by Scanning Electron Microscopy (SEM) for micromorphological analysis using a JEOL JSM-6400 (JEOL, Tokyo, Japan) equipped with an INCA EDX detector X-sight Series Si (Li) Oxford pentaFET microanalysis system. The samples were coated with carbon before analyses.

Thermogravimetric analysis (TGA) was performed using a TA SDT 2960 TG-DSC simultaneous instrument. Pt crucibles containing 5–7 mg of the sample were heated at 2 °C min^{-1} from room temperature to 1000 °C under a dry oxidizing atmosphere.

In addition, Micro-Raman analysis was carried out by means of a Renishaw inVia confocal microRaman spectrometer (Renishaw, Gloucestershire, UK) coupled to a DMLM Leica microscope provided with 5×, 20×, 50× and 100× long working distance lenses using a 785 nm (NIR) excitation laser. The laser was set at low power (not more than 1 mW at the sample) in order to avoid thermal photodecomposition. Data acquisition was carried out using Renishaw's WireTM 3.2 software package. The interpretation of Raman results was carried out by comparison of acquired Raman spectra with Raman spectra of pure standard compounds collected in the e-VISNICH dispersive Raman database.

Finally, Fourier transform infrared (ATR FT-IR) spectroscopy was carried out to determine the phase nature of the binder using an Agilent 4300 Handheld FTIR Spectrometer (Agilent, Santa Clara, CA, USA) with the diamond attenuated total reflectance (ATR) sampling module and acquiring spectra in the absorbance mode between 650 and 4000 cm^{-1}. Sixty-four scans per spectrum were collected using a resolution of 4 cm^{-1}.

The pore size distribution and the open porosity (PMIP) were determined by mercury intrusion porosimetry (MIP) using a Poremaster-60 GT porosimeter (Quantachrome Instruments, Boynton Beach, FL, USA), measuring the pore diameter in a range of 0.003 µm to 100 µm. Mortar fragments of ca. 1 cm^3 were oven-dried for 24 h at 60 °C before the analysis.

The aesthetic compatibility of a repair mortar with the original is an important requirement in the restoration of historic buildings [43,44]. The color of samples was measured by spectrophotometry according to the CIELAB (CIE 1976 L*a*b*) color space system proposed by the International Commission on Illumination (CIE) following the UNE-EN 15,886 standard [45]. The lightness (L*) and chromatic (a* and b*) parameters were obtained using a Konica-Minolta CR-400 portable Chroma Meter (Konica Minolta Inc, Osaka, Japan) on an area 8 mm in diameter, viewing vertically under 0°, using D65 standard illuminant, with SCI mode and a 400–700 nm wavelength range. Color measurements were performed at ten different points of each mortar sample, and the mean value was calculated.

3. Results

3.1. Textural Characterization

Microscopically, all lime mortar samples show a heterogeneous binder matrix-supported microtexture, with siliceous aggregates of metamorphic a nature embedded in a micritic binder matrix. The mortars show different binder/aggregate ratios, ranging from 1/3 to 1/2 in the mortars from the foundations (sample ARC-2 and sample ARC-1, respectively) and 1/1 in the mortar from the intrados of the Mudejar arch (ARC-3) (Figure 2a–c). All mortars show heterometric lime lumps and some charcoal fragments dispersed in the binder matrix, mainly in sample ARC-1 (Figure 2d). However, textural differences between the mortars were observed. Sample ARC-1 shows sub-rounded quartz grains as aggregates, ranging from 0.1 mm up to 1.25 mm in size, and shows a deteriorated texture, with large secondary pores up to 1 mm coated with secondary calcite crystals (Figure 2a). Unlike sample ARC-1, the aggregates of sample ARC-2 are poorly sorted and consist of larger sub-rounded quartz grains up to 2 mm in size and sub-rounded quartzite rock fragments up to 2.5 mm in size. Pyrite and phyllosilicate crystals were also observed dispersed in the binder matrix. Similarly, sample ARC-3 consists of sub-rounded quartz and quartzite rock fragment aggregates, but smaller in size, with quartz grains and quartzite rock fragments up to 1 mm.

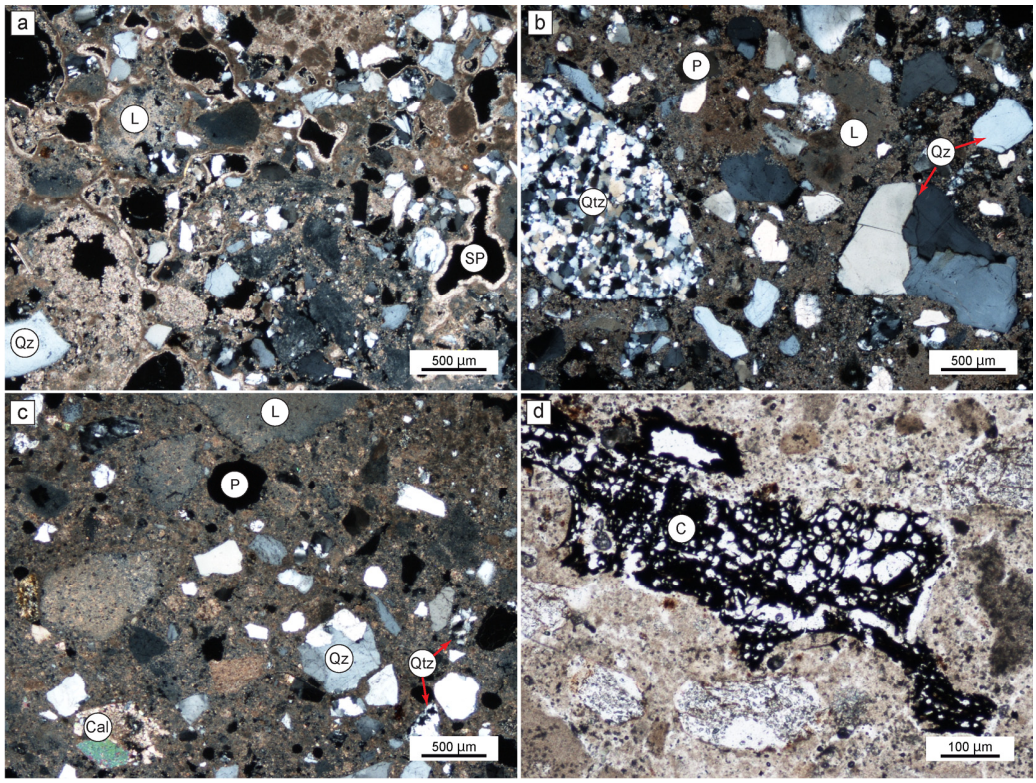

Figure 2. Photomicrographs of the lime mortars from the Arch of San Martin. (**a**) ARC-1 mortar, (**b**) ARC-2 mortar, (**c**) ARC-3 showing a heterogeneous binder matrix-supported texture with silicate aggregates embedded in a micritic calcite matrix (XPL). (**d**) Charcoal fragments dispersed in the matrix (PPL). Abbreviations: Qtz: quartzite; Qz: quartz; L: lime lump; Cal: calcite; C: charcoal; P: pore; SP: secondary porosity; PPL: plane-polarized light; XPL: cross-polarized light.

3.2. Mineralogical and Chemical Characterization

The bulk fraction (BF) of all mortar samples is mainly composed of calcite and quartz, with varying proportions among the samples (Table 2). A minor amount of potassium feldspar was also detected in sample ARC-1, and muscovite-like phyllosilicates in sample ARC-2. The sample ARC-3 mortar is the richest in calcite, with minor amounts of potassium feldspar, muscovite-like phyllosilicates and gypsum.

Table 2. Mineralogy of the bulk and extracted binder fractions of the Arch of San Martin lime mortars.

Sample	Calcite	Quartz	K-Feldspar	Phyllosilicates	Other Phases
ARC-1 BF	**	****	tr		
ARC-2 BF	*	****		tr	
ARC-3 BF	****	****	tr	tr	tr (gypsum)
Binder					
ARC-1 < 20 µm	****	*		tr	
ARC-2 < 20 µm	****	*		*	tr (dolomite) tr (amesite)
ARC-3 < 20 µm	****	tr			
ARC-1 < 2 µm	****	tr		tr	
ARC-2 < 2 µm	****	tr		*	tr (amesite)
ARC-3 < 2 µm	****				tr (gypsum)

****: very abundant; **: low abundance; *: very low abundance; tr: trace amount.

As expected, the extracted binder fractions are mainly composed of calcite, with minor amounts of quartz and traces of phyllosilicates from aggregates (Table 2). The

minor mineral content decreases or even disappears as the particle grain size decreases. In the fraction <20 µm of sample ARC-2, traces of dolomite and amesite were also detected (Figure 3). In binder fraction <2 µm, amesite was also detected in sample ARC-2, whereas in sample ARC-3, traces of gypsum were detected. Amesite, a phyllosilicate-like magnesium aluminosilicate (M-A-S-H) phase with the general formula $Mg_2Al_2SiO_5OH_4$, was identified according to broad peaks at ~12.5 °2θ and ~25 °2θ, and the XDR pattern suggests a low degree of crystallinity. The SEM image of the ARC-3 sample shows the characteristic texture of gypsum crystals (Figure 4a), whereas in the SEM image of the ARC-2 sample (Figure 4b), the amesite is characterized by the lacy forms of magnesium-aluminum hydrate silicates; the main chemical composition is determined by EDS analysis.

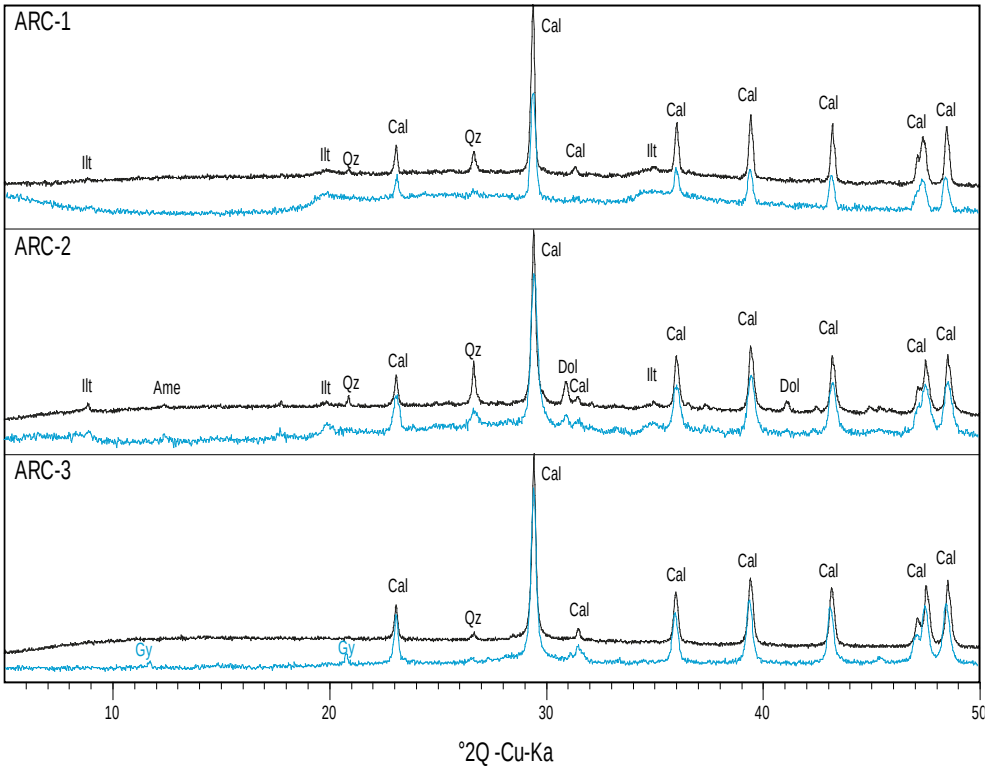

Figure 3. XRD spectra showing the mineralogy of the binder fractions of the Arch of San Martin mortars. The binder fraction <2 µm is shown in blue (bottom), and the binder fraction <20 µm is shown in black (top) Abbreviations: Ilt: Illite; Qz: Quartz; Cal: Calcite; Dol: Dolomite; Ame: Ameste; Gy; Gypsum.

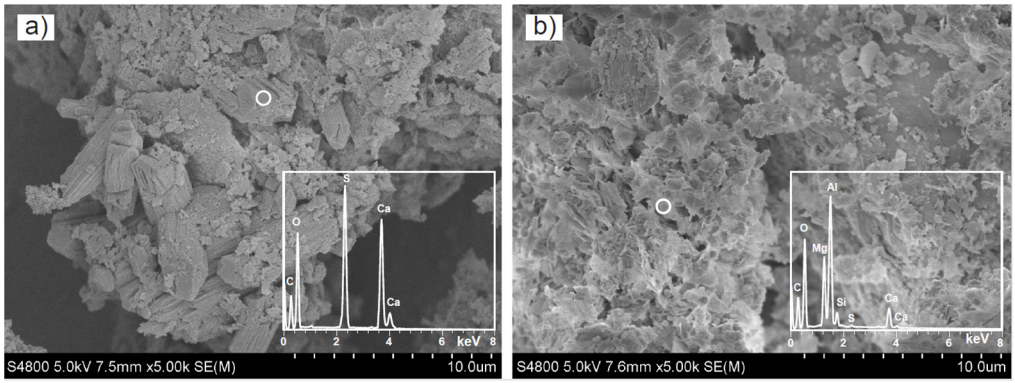

Figure 4. Scanning electron microscopy image: (**a**) gypsum crystals in sample ARC-3; (**b**) lacy amesite crystals in sample ARC-2 and EDS analysis. Circles mark EDS analysis point.

Chemical analyses were determined in the bulk mortar and in the binder fractions <20 μm and <2 μm (Table 3). The chemical composition is consistent with the mineral phases identified by XRD. High SiO_2 values in the bulk fractions are related with silicates such as quartz, phyllosilicates and feldspars. In fact, mortar ARC-2 shows the highest SiO_2 value (74.4 wt%) corresponding to a quartz-enriched sample and the lowest CaO values (7.2 wt%). The Al_2O_3, MgO and TiO_2 contents are related to the amounts of phyllosilicate and feldspar. On the contrary, mortar ARC-3 shows the lowest SiO_2 value (29.9 wt%) and the highest CaO (35.7 wt%) and LOI (28.9 wt%) values, corresponding to a higher amount of calcite.

Table 3. Chemical composition of major elements of the bulk lime mortar and binder fractions expressed as oxides in wt %.

	SiO_2	Al_2O_3	Fe_2O_3	MgO	CaO	K_2O	TiO_2	P_2O_5	SO_3	LOI	Total
ARC-1 BF	55.48	0.98	0.28	0.41	19.33	0.44	0.08	0.18	0.31	20.03	97.52
ARC-2 BF	74.35	1.97	0.48	1.31	7.22	0.56	0.18	0.05	0.13	10.2	96.45
ARC-3 BF	29.9	0.88	0.29	0.47	35.67	0.34	0.08	0.06	0.8	28.94	97.43
ARC1 < 20 μm	13.77	4.4	1.41	2.49	35.17	0.91	0.18	0.41	0.49	39.67	98.9
ARC2 < 20 μm	23.2	4.22	1.31	7.44	25.47	0.74	0.14	0.28	0.82	35.33	98.95
ARC3 < 20 μm	3.23	0.96	0.4	0.82	44.26	0.23	0.04	0.09	0.29	48.98	99.3
ARC-1 < 2 μm	1.53	0.54	0.34	0.30	53.64	0.14	0.12	0.14	0.49	42.15	99.39
ARC-2 < 2 μm	2.52	0.57	0.23	0.84	52.76	0.12	0.21	0.23	0.20	41.46	99.15
ARC-3 < 2 μm	0.52	0.30	0.14	0.28	54.78	0.07	0.05	0.11	0.89	43.04	100.19

LOI: loss on ignition (%).

The extraction processes of the different binder fractions involve the progressive removal of the aggregate components of the mortar, thereby affecting the chemical composition of the fractions. Thus, the fractions <20 μm show CaO contents ranging from 25.5 wt% to 44.3 wt%, whereas the fractions <2 μm show CaO contents ranging between 52.8 wt% and 54.8 wt% due to the enrichment in calcite in the finer fraction. The SiO_2, Al_2O_3 and MgO contents are related to the amounts of phyllosilicate-like phases (i.e., illite and/or amesite). The 0.89 wt% SO_3 content in the binder fraction of ARC-2 is related to the presence of gypsum.

Thermal analysis (TGA) was performed to further characterize the binder. In general, the TGA analyses agree with the XRD results, showing an intense weight loss in the temperature range 650–800 °C, attributed to the decarbonation of calcite (Figure 5). In particular, binder fractions of sample ARC-1 and sample ARC-2 show 3% and 7% weight loss at 120 °C, respectively, attributed to water desorption. The weight loss (ca. 6.5%) from 120 °C to 600 °C is attributed to the dehydration of hydroxyl groups (OH−) of phyllosilicate phases (illite) and hydraulic components (amesite) as well as the decomposition of organic matter. The weight loss in the temperature range of 650–800 °C is 22% for sample ARC-1, 9% for sample ARC-2 and 32% for sample ARC-3.

Raman spectroscopy analyses of the binders allow characterization of the organic matter. The Raman spectra of the organic matter show two characteristic first-order bands at about 1350 cm^{-1} and 1600 cm^{-1}, assigned to carbonaceous matter. Figure 6 shows the representative spectrum of each mortar. Two broad bands with intensity maxima at approximately 1590 cm^{-1} corresponding to band G and 1340 cm^{-1} corresponding to band D were observed. However, each spectrum showed distinctive features. The spectra of sample ARC-1 and sample ARC-2 show broad bands, whereas the spectrum of sample ARC-3 shows narrow bands. The relative intensity and width of the bands are sensitive to the degree of disorder or crystallinity of the carbon materials and change significantly with temperature [46,47].

The ATR FT-IR spectra of the binders were very similar and correspond mainly to phyllosilicates and carbonate functional groups (Figure 7). All samples showed bands at around 713 cm^{-1}, 875 cm^{-1} and 1425 cm^{-1}, attributed to calcite. A band present in the

binder of sample ARC-1 and sample ARC-3 around 1000 cm^{-1} was attributed to quartz. The band at approximately 980 cm^{-1} and a broad band between 3100 cm^{-1} and 3700 cm^{-1} in sample ARC-2 were attributed to the amesite phase. Similarly, although amesite was not determined by XRD, the presence of amesite in sample ARC-1 was confirmed on the basis of the broad band between 3100 cm^{-1} and 3700 cm^{-1}. The detection limits of each analytical technique and the small amount of amesite in sample ARC-1 explain the difference between the XRD and ATR FT-IR results. Gypsum in ARC-1 was also identified by weak bands at 1100 cm^{-1} and 3434 cm^{-1}.

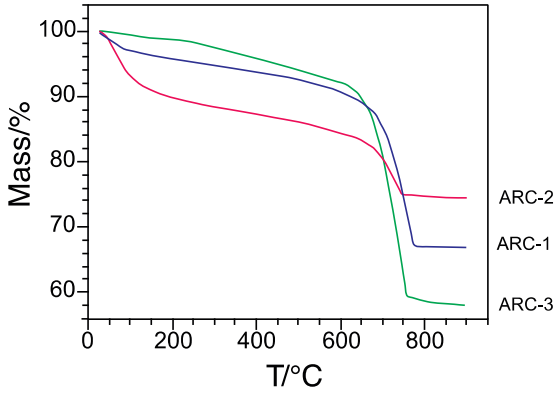

Figure 5. Thermogravimetric analyses of the binder fraction of lime mortar from the Arch of San Martin.

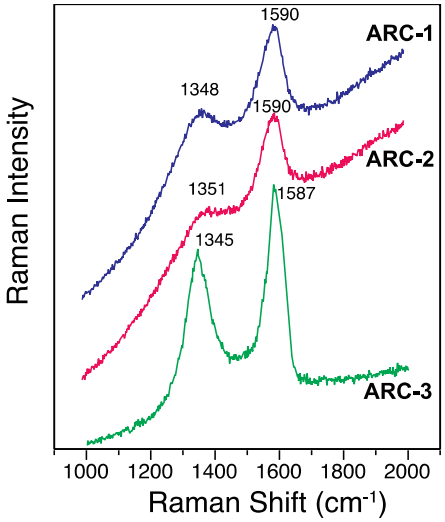

Figure 6. Micro-Raman spectra of organic matter in mortar from the Arch of San Martin.

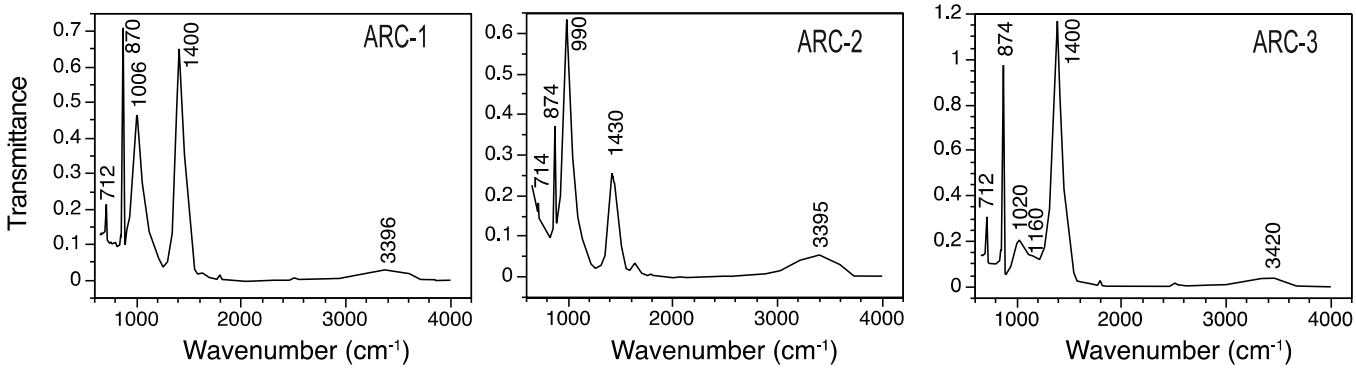

Figure 7. FT-IR spectra of the binder fraction of Arch of San Martin mortar.

3.3. Physical Characterization

The highest porosity values obtained by mercury intrusion porosimetry (PMIP) were measured in sample ARC-1 and sample ARC-2 (48.94% and 45.42%, respectively), whereas the lowest value was measured in sample ARC-3 (44.86%). The pore size of mortars shows a large volume of small pores (0.01 < r < 1 μm) connected to larger pores (1 < r < 10 μm), with a greater volume of pores in the range 0.1 < r < 1 μm. Sample ARC-1 shows a nearly unimodal pore size distribution, ranging between 0.01 μm and 1 μm and with a main peak at around 0.2 μm (Figure 8a). Sample ARC-2 shows a more heterogeneous pore size distribution, with three main peaks at around 0.03 μm, 0.4 μm and 7 μm, respectively (Figure 8b). Sample ARC-3 shows a nearly unimodal pore size distribution of large pores of between 0.01 and 1 μm, with a main peak at 0.4 μm, and a large tail of a second smaller family of pores ranging between 1 μm and 20 μm in size (Figure 8c). The pore size distribution obtained for both sample ARC-2 and sample ARC-3 could indicate the presence of coarse quartzite rock fragments in the measurement.

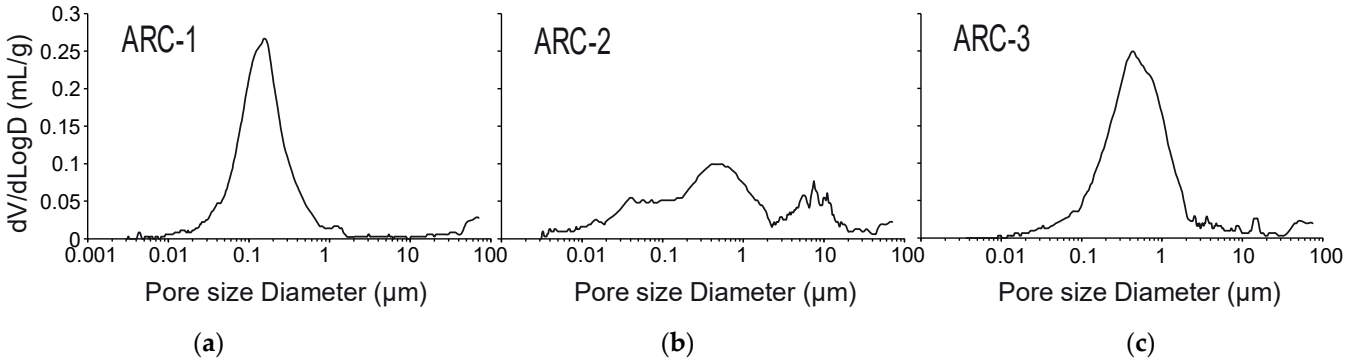

Figure 8. Pore size distribution curves of lime mortars from the Arch of San Martin obtained by mercury intrusion porosimetry (MIP). (**a**) Sample ARC-1. (**b**) sample ARC-2. (**c**) sample ARC-3.

The chromatic parameters of each mortar sample are summarized in Table 4. The lightness (L*) values around 80 and the values measured for the chromatic axes (a* and b*) indicated samples with a tendency toward the light grey field. The lower L* value and higher a* and b* values measured in sample ARC-2 were explained by the presence of phyllosilicate.

Table 4. Chromatic parameters of the lime mortars from the Arch of San Martin.

Sample	L*	a*	b*	C*	H
ARC-1	81.14	3.08	7.83	8.41	68.53
ARC-2	80.45	3.81	10.85	11.50	70.66
ARC-3	84.50	1.54	8.77	8.90	80.37

L*: Lightness; a* and b*: chromatic coordinates; C*: chroma; H: hue angle.

4. Discussion

The mineralogical and chemical characterization of the mortar provides information on the construction history of the building and gives clues as to the production of the historic mortars. In this respect, the foundation mortars show differences in both the nature of the aggregates and the binder/aggregate ratios. In addition, the lime used in the manufacture of the foundation mortars was also different, as the chemical composition of the binder reflects.

The amesite M-A-S-H phase detected in sample ARC-1 and sample ARC-2 point to the use of magnesium-rich limestones or impure limestones containing clay minerals or other silicates for mortar manufacturing. However, the higher amount of amesite in ARC-2 and the presence of dolomite suggest the use of dolomitic limestone in the manufacture of mortar in the intermediate phase.

Magnesium silicate hydrated phases are formed during the hydration of Mg-bearing lime by the reaction of silicates and dolomite in a chemical environment with available aluminum. However, this not only depends on the binder chemistry (i.e., magnesium limes) but also on several factors triggering chemical reaction. Saltwater or other alkaline media and/or the presence of certain aggregates and clay minerals, usually stable under normal conditions, can develop para-pozzolanic phases [48,49]. Amesite constitutes a hydraulic phase, contributing to a decrease in the porosity and favoring the waterproofing behavior of mortar [50–56].

A less porous material is more resistant to deterioration when exposed to groundwater. The variation in the mineralogical composition of the lime used in the manufacture of foundation mortars suggests a deliberate selection of the raw material according to the high-humidity conditions of the foundation environment. Thus, the differences between the foundation mortars suggest a technological improvement in the manufacture of mortars according to the specific construction requirements. The mortars of the intrados of the Mudejar arch (Sample ARC-3) show a higher binder/aggregate ratio (1/1) than the mortars from the foundation. The absence of silicate phases in the mortar of the intrados indicates that the lime was produced from pure limestone. The presence of gypsum in sample ARC-3 is due to the presence of sulphates from the urban air pollution, as the Arch of San Martin was until recently an area of road traffic.

Chemical and mineralogical characterization of the binder fractions allowed determination of the most suitable sample for mortar radiocarbon dating. The dolomite identified in the binder of sample ARC-2 (Figure 3) could incorporate dead carbon into the system, leading to an overestimation of the age; therefore, the sample is excluded from radiocarbon dating. In sample ARC-1, secondary calcite coats the secondary porosity of the mortar (Figure 2a). Secondary carbonates are precipitated by the interaction with groundwater or rainwater, containing variable amounts of dissolved inorganic and/or organic carbon, resulting in either underestimated ages or overestimated ages [57], making sample ARC-1 also unsuitable for radiocarbon dating. Although the binder of the sample ARC-3 is mainly composed of calcite, the presence of charcoal fragments (Figures 2d and 6) also precludes this sample from radiocarbon dating.

5. Conclusions

The mineralogical and chemical characterization of the lime mortars studied reveals differences among the mortars from the foundation and the intrados of the Arch of San Martin The differences are related to the nature of aggregates and the binder/aggregate ratio. The chemical composition of the binder of sample ARC-3 suggests pure limestone was used to produce the lime for the intrados mortar. In the foundation mortar, traces of amesite were identified, and the higher contents of alumina and magnesia in the binder suggest impure limestone was used for the lime of ARC-1 and ARC-2 mortars.

The presence of microparticles of charcoal, dolomite and secondary calcite, considered contaminants in mortar radiocarbon dating, preclude the mortars from the Arch of San Martin from radiocarbon dating.

The data obtained from this research provide only limited information on the building phases of the Arco de San Martín. In order to better understand the construction phases of the building and to obtain information on the raw materials used in the mixtures and the manufacturing technology of the mortars, more extensive sampling is required. Unfortunately, this is not easily feasible, considering that the monument is strictly protected as an Asset of Cultural Interest.

Author Contributions: Conceptualization, M.C.Z., L.Á.O. and G.P.-A.; methodology, G.P.-A., M.C.Z. and L.Á.O.; investigation, G.P.-A., M.C.Z. and L.Á.O.; resources, G.P.-A., M.C.Z., L.Á.O., J.J.E. and C.A.F.; writing—original draft preparation, G.P.-A. and M.C.Z.; writing—review and editing, M.C.Z., L.Á.O. and G.P.-A.; funding acquisition, M.C.Z., L.Á.O. and G.P.-A. All authors have read and agreed to the published version of the manuscript.

Funding: This research was funded by the Basque Country Government, grant number IT1442-22.

Data Availability Statement: The data is contained within the article.

Acknowledgments: G.P.-A. acknowledges the Margarita Salas Postdoctoral Fellowship (MARSA21/57) founded by the European Union—NextGenerationEU and the Spanish Ministry of Universities. The authors would also like to thank to the two anonymous referees for their suggestions, which improved the manuscript. Also, the authors would like to thank Peter Smith for reviewing the use of English in the manuscript.

Conflicts of Interest: Authors Javier Jiménez Echevarría and Carmen Alonso Fernández are employees of Cronos S.C. Arqueología y Patrimonio. The paper reflects the views of the scientists and not the company.

References

1. Secco, M.; Previato, C.; Addis, A.; Zago, G.; Kamsteeg, A.; Dilaria, S.; Canovaro, C.; Artioli, G.; Bonetto, J. Mineralogical clustering of the structural mortars from the Sarno Baths, Pompeii: A tool to interpret construction techniques and relative chronologies. *J. Cult. Herit.* **2019**, *40*, 265–273. [CrossRef]
2. Chiarelli, N.; Miriello, D.; Bianchi, G.; Fichera, G.; Giamello, M.; Memmi, I.T. Characterisation of ancient mortars from the S. Niccolò archaeological complex in Montieri (Tuscany–Italy). *Constr. Build. Mater.* **2015**, *96*, 442–460. [CrossRef]
3. Lezzerini, M.; Raneri, S.; Pagnotta, S.; Columbu, S.; Gallello, G. Archaeometric study of mortars from the Pisa's Cathedral Square (Italy). *Measurement* **2018**, *126*, 322–331. [CrossRef]
4. Gheris, A. New dating approach based on the petrographical, mineralogical and chemical characterization of ancient lime mortar: Case study of the archaeological site of Hippo, Annaba city, Algeria. *Herit. Sci.* **2023**, *11*, 103. [CrossRef]
5. Miriello, D.; Bloise, A.; Crisci, G.M.; De Luca, R.; De Nigris, B.; Martellone, A.; Osanna, M.; Pace, R.; Pecci, A.; Ruggieri, N. New compositional data on ancient mortars and plasters from Pompeii (Campania–Southern Italy): Archaeometric results and considerations about their time evolution. *Mater. Charact.* **2018**, *146*, 189–203. [CrossRef]
6. Miriello, D.; Barca, D.; Bloise, A.; Ciarallo, A.; Crisci, G.M.; De Rose, T.; Gattuso, C.; Gazineo, F.; La Russa, M.F. Characterisation of archaeological mortars from Pompeii (Campania, Italy) and identification of construction phases by compositional data analysis. *J. Archaeol. Sci.* **2010**, *37*, 2207–2223. [CrossRef]
7. De Luca, R.; Miriello, D.; Pecci, A.; Domínguez-Bella, S.; Bernal-Casasola, D.; Cottica, D.; Bloise, A.; Crisci, G.M. Archaeometric Study of Mortars from the Garum Shop at Pompeii, Campania, Italy. *Geoarchaeology* **2015**, *30*, 330–351. [CrossRef]
8. Dilaria, S.; Previato, C.; Secco, M.; Busana, M.S.; Bonetto, J.; Cappellato, J.; Ricci, G.; Artioli, G.; Tan, P. Phasing the history of ancient buildings through PCA on mortars' mineralogical profiles: The example of the Sarno Baths (Pompeii). *Archaeometry* **2022**, *64*, 866–882. [CrossRef]
9. Carò, F.; Riccardi, M.; Mazzilli Savini, M. Characterization of plasters and mortars as a tool in archaeological studies: The case of Lardirago Castle in Pavia, Northern Italy. *Archaeometry* **2008**, *50*, 85–100. [CrossRef]
10. Genestar, C.; Pons, C.; Más, A. Analytical characterisation of ancient mortars from the archaeological Roman city of Pollentia (Balearic Islands, Spain). *Anal. Chim. Acta* **2006**, *557*, 373–379. [CrossRef]
11. Miriello, D.; Barca, D.; Pecci, A.; De Luca, R.; Crisci, G.M.; López Luján, L.; Barba, L. Plasters from Different Buildings of the Sacred Precinct of Tenochtitlan (Mexico City): Characterization And Provenance. *Archaeometry* **2015**, *57*, 100–127. [CrossRef]
12. Alonso-Olazabal, A.; Ortega, L.A.; Zuluaga, M.C.; Ponce-Antón, G.; Jiménez Echevarría, J.; Alonso Fernández, C. Compositional characterization and chronology of roman mortars from the archaeological site of arroyo de la dehesa de velasco (Burgo de osma-ciudad de osma, Soria, Spain). *Minerals* **2020**, *10*, 393. [CrossRef]
13. TC 203-RHM (Jan Erik Lindqvist). Rilem TC 203-RHM: Repair mortars for historic masonry. Testing of hardened mortars, a process of questioning and interpreting. *Mater. Struct.* **2009**, *42*, 853–865. [CrossRef]
14. Anna, A.; Giuseppe, C. The water transfer properties and drying shrinkage of aerial lime-based mortars: An assessment of their quality as repair rendering materials. *Environ. Earth Sci.* **2014**, *71*, 1699–1710. [CrossRef]
15. Hughes, J.J.; Cuthbert, S.J. The petrography and microstructure of medieval lime mortars from the west of Scotland: Implications for the formulation of repair and replacement mortars. *Mater. Struct.* **2000**, *33*, 594–600. [CrossRef]
16. Morillas, H.; Vazquez, P.; Maguregui, M.; Marcaida, I.; Silva, L.F.O. Composition and porosity study of original and restoration materials included in a coastal historical construction. *Constr. Build. Mater.* **2018**, *178*, 384–392. [CrossRef]
17. Nogueira, R.; Ferreira Pinto, A.P.; Gomes, A. Design and behavior of traditional lime-based plasters and renders. Review and critical appraisal of strengths and weaknesses. *Cem. Concr. Compos.* **2018**, *89*, 192–204. [CrossRef]
18. Lanas, J.; Alvarez-Galindo, J.I. Masonry repair lime-based mortars: Factors affecting the mechanical behavior. *Cem. Concr. Res.* **2003**, *33*, 1867–1876. [CrossRef]
19. Al-Bashaireh, K. Reconstructing the Chronology of the House XVII-XVIII Complex at Umm el-Jimal, East Jordan: Radiocarbon Dates of Organic Inclusions of Architectural Mortars. *Radiocarbon* **2014**, *56*, 245–256. [CrossRef]
20. Al-Bashaireh, K. Radiocarbon Age Determinations of Mosaic Mortar Layers of Churches from North Jordan. *Radiocarbon* **2015**, *57*, 851–863. [CrossRef]

21. Al-Bashaireh, K.; Hodgins, G.W.L. AMS 14C dating of organic inclusions of plaster and mortar from different structures at Petra-Jordan. *J. Archaeol. Sci.* **2011**, *38*, 485–491. [CrossRef]
22. Nawrocka, D.M.; Michczynska, D.J.; Pazdur, A.; Czernik, J. Radiocarbon chronology of the ancient settlement in the Golan Heights area, Israel. *Radiocarbon* **2007**, *49*, 625–637. [CrossRef]
23. Pachnerová Brabcová, K.; Kundrát, P.; Krofta, T.; Suchý, V.; Petrová, M.; John, D.; Kozlovcev, P.; Kotková, K.; Fialová, A.; Kubančák, J.; et al. Extensive Survey on Radiocarbon Dating of Organic Inclusions in Medieval Mortars in the Czech Republic. *Radiocarbon* **2023**, *2023*, 1–11. [CrossRef]
24. Pachnerová Brabcová, K.; Kundrát, P.; Krofta, T.; Suchý, V.; Petrová, M.; Pravdíková, N.; John, D.; Kozlovcec, P.; Kotková, K.; Fialová, A.; et al. Radiocarbon Dating of Mortar Charcoals from Medieval RÝzmburk Castle, Northwestern Bohemia. *Radiocarbon* **2022**, *65*, 275–283. [CrossRef]
25. Schiffer, M.B. Radiocarbon dating and the "old wood" problem: The case of the Hohokam chronology. *J. Archaeol. Sci.* **1986**, *13*, 13–30. [CrossRef]
26. Berger, R. 14C Dating Mortar in Ireland. *Radiocarbon* **1992**, *34*, 880–889. [CrossRef]
27. Berger, R. Radiocarbon dating of early medieval Irish monuments. In *Proceedings of the Royal Irish Academy. Section C: Archaeology, Celtic Studies, History, Linguistics, Literature*; Royal Irish Academy: Dublin, Ireland, 1995; pp. 159–174.
28. Marzaioli, F.; Lubritto, C.; Nonni, S.; Passariello, I.; Capano, M.; Terrasi, F. Mortar radiocarbon dating: Preliminary accuracy evaluation of a novel methodology. *Anal. Chem.* **2011**, *83*, 2038–2045. [CrossRef]
29. Lindroos, A.; Heinemeier, J.; Ringbom, Å.; Braskén, M.; Sveinbjörnsdóttir, Á. Mortar dating using AMS 14C and sequential dissolution: Examples from medieval, non-hydraulic lime mortars from the Åland Islands, SW Finland. *Radiocarbon* **2007**, *49*, 47–67. [CrossRef]
30. Ortega, L.A.; Zuluaga, M.C.; Alonso-Olazabal, A.; Murelaga, X.; Insausti, M.; Ibañez-Etxeberria, A. Historic lime-mortar 14C dating of Santa María la real (Zarautz, Northern Spain): Extraction of suitable grain size for reliable 14C dating. *Radiocarbon* **2012**, *54*, 23–36. [CrossRef]
31. Ponce-Antón, G.; Ortega, L.A.; Zuluaga, M.C.; Alonso-Olazabal, A.; Solaun, J.L. Hydrotalcite and hydrocalumite in mortar binders from the medieval castle of portilla (Álava, North Spain): Accurate mineralogical control to achieve more reliable chronological ages. *Minerals* **2018**, *8*, 326. [CrossRef]
32. Pesce, G.; Quarta, G.; Calcagnile, L.; D'Elia, M.; Cavaciocchi, P.; Lastrico, C.; Guastella, R. Radiocarbon dating of lumps from aerial lime mortars and plasters: Methodological issues and results from San Nicolò of Capodimonte Church (Camogli, Genoa, Italy). *Radiocarbon* **2009**, *51*, 867–872. [CrossRef]
33. Hajdas, I.; Lindroos, A.; Heinemeier, J.; Ringbom, A.; Marzaioli, F.; Terrasi, F.; Passariello, I.; Capano, M.; Artioli, G.; Addis, A.; et al. Preparation and Dating of Mortar Samples-Mortar Dating Inter-Comparison Study (MODIS). *Radiocarbon* **2017**, *59*, 1845–1858. [CrossRef]
34. Addis, A.; Secco, M.; Marzaioli, F.; Artioli, G.; Arnau, A.C.; Passariello, I.; Terrasi, F.; Brogiolo, G.P. Selecting the Most Reliable 14C Dating Material Inside Mortars: The Origin of the Padua Cathedral. *Radiocarbon* **2019**, *61*, 375–393. [CrossRef]
35. Warner, R.B. A Proposed Adjustment for the 'Old-Wood Effect'. In *Proceedings of the 2nd Symposium of ^{14}C & Archaeology*; Mook, W., Waterbolk, H., Eds.; European Science Foundation (ESF): Groningen, The Netherlands, 1987; pp. 159–172.
36. Caroselli, M.; Hajdas, I.; Cassitti, P. The Dating of Dolomitic Mortars with Uncertain Chronology from MÜstair Monastery: Sample Characterization and Combined Interpretation of Results. *Radiocarbon* **2023**, *2023*, 1–13. [CrossRef]
37. Ricci, G.; Secco, M.; Addis, A.; Pistilli, A.; Preto, N.; Brogiolo, G.P.; Arnau, A.C.; Marzaioli, F.; Passariello, I.; Terrasi, F.; et al. Integrated multi-analytical screening approach for reliable radiocarbon dating of ancient mortars. *Sci. Rep.* **2022**, *12*, 3339. [CrossRef] [PubMed]
38. Marzaioli, F.; Nonni, S.; Passariello, I.; Capano, M.; Ricci, P.; Lubritto, C.; De Cesare, N.; Eramo, G.; Quirós Castillo, J.A.; Terrasi, F. Accelerator mass spectrometry 14C dating of lime mortars: Methodological aspects and field study applications at CIRCE (Italy). *Nucl. Instrum. Methods Phys. Res. Sect. B Beam Interact. Mater. At.* **2013**, *294*, 246–251. [CrossRef]
39. Folk, R.L.; Valastro, S. Successful technique for dating of lime mortar by carbon-14. *J. Field Archaeol.* **1976**, *3*, 203–208. [CrossRef]
40. Nawrocka, D.; Czernik, J.; Goslar, T. 14C dating of carbonate mortars from polish and Israeli sites. *Radiocarbon* **2009**, *51*, 857–866. [CrossRef]
41. Heinemeier, J.; Ringbom, Å.; Lindroos, A.; Sveinbjörnsdóttir, Á.E. Successful AMS 14C dating of non-hydraulic lime mortars from the medieval churches of the Åland Islands, Finland. *Radiocarbon* **2010**, *52*, 171–204. [CrossRef]
42. Folk, R.L. A comparison chart for visual percentage estimation. *J. Sediment. Res.* **1951**, *21*, 32–33.
43. López, A.; Guzmán, G.A.; Di Sarli, A.R. Color stability in mortars and concretes. Part 1: Study on architectural mortars. *Constr. Build. Mater.* **2016**, *120*, 617–622. [CrossRef]
44. Schueremans, L.; Cizer, Ö.; Janssens, E.; Serré, G.; Balen, K.V. Characterization of repair mortars for the assessment of their compatibility in restoration projects: Research and practice. *Constr. Build. Mater.* **2011**, *25*, 4338–4350. [CrossRef]
45. *UNE-EN 15886:2011*; Conservation of Cultural Property. Test Methods. Colour Measurement of Surfaces: Madrid, Spain, 2011.
46. Sadezky, A.; Muckenhuber, H.; Grothe, H.; Niessner, R.; Pöschl, U. Raman microspectroscopy of soot and related carbonaceous materials: Spectral analysis and structural information. *Carbon* **2005**, *43*, 1731–1742. [CrossRef]
47. Pawlyta, M.; Rouzaud, J.N.; Duber, S. Raman microspectroscopy characterization of carbon blacks: Spectral analysis and structural information. *Carbon* **2015**, *84*, 479–490. [CrossRef]

48. Bernard, E.; Nguyen, H.; Kawashima, S.; Lothenbach, B.; Manzano, H.; Provis, J.; Scott, A.; Unluer, C.; Winnefeld, F.; Kinnunen, P. MgO-based cements—Current status and opportunities. *RILEM Tech. Lett.* **2023**, *8*, 65–78. [CrossRef]
49. Dilaria, S.; Secco, M.; Bonetto, J.; Ricci, G.; Artioli, G. Making Ancient Mortars Hydraulic. How to Parametrize Type and Crystallinity of Reaction Products in Different Recipes. In *Conservation and Restoration of Historic Mortars and Masonry Structures*; Springer: Cham, Switzerland, 2023; pp. 36–52.
50. Papayianni, I.; Stefanidou, M. Strength–porosity relationships in lime–pozzolan mortars. *Constr. Build. Mater.* **2006**, *20*, 700–705. [CrossRef]
51. Thomson, M.; Lindqvist, J.; Elsen, J.; Groot, C. 2.5 Porosity of Mortars. In *Characterisation of Old Mortars with Respect to their Repair*; Final Report of RILEM TC 167-COM; Groot, C., Ashall, G., Hughes, J., Eds.; RILEM Publications SARL: Champs-sur-Marne, France, 2004; Volume 28, pp. 77–106.
52. Ponce-Antón, G.; Zuluaga, M.C.; Ortega, L.A.; Agirre Mauleon, J. Petrographic and Chemical–Mineralogical Characterization of Mortars from the Cistern at Amaiur Castle (Navarre, Spain). *Minerals* **2020**, *10*, 311. [CrossRef]
53. Shafer, J.; Hilsdorf, H. Ancient and new lime mortars—The correlation between their composition, structure and mechanical properties. In Proceedings of the International Congress on Conservation of Stone and Other Materials, E & FN Spon, Paris, France, 29 June–1 July 1993; pp. 605–612.
54. Papayianni, I.; Stefanidou, M. The evolution of porosity in lime based mortars. In Proceedings of the 8th Euroseminar on Microscopy Applied to Building Materials, Athens, Greece, 4–7 September 2001; pp. 4–7.
55. Silva, A.S.; Gameiro, A.; Grilo, J.; Veiga, R.; Velosa, A. Long-term behavior of lime–metakaolin pastes at ambient temperature and humid curing condition. *Appl. Clay Sci.* **2014**, *88–89*, 49–55. [CrossRef]
56. Bernard, E.; Lothenbach, B.; Cau-Dit-Coumes, C.; Chlique, C.; Dauzères, A.; Pochard, I. Magnesium and calcium silicate hydrates, Part I: Investigation of the possible magnesium incorporation in calcium silicate hydrate (C-S-H) and of the calcium in magnesium silicate hydrate (M-S-H). *Appl. Geochem.* **2018**, *89*, 229–242. [CrossRef]
57. Nawrocka, D.; Michniewicz, J.; Pawlyta, J.; Pazdur, A. Application of radiocarbon method for dating of lime mortars. *Geochronometria* **2005**, *24*, 109–115.